First-principles simulation of Raman spectra and structural properties of quartz up to 5 GPa*

Liu Lei(刘 雷)[a)†], Lv Chao-Jia(吕超甲)[a)], Zhuang Chun-Qiang(庄春强)[b)], Yi Li(易 丽)[a)], Liu Hong(刘 红)[a)], and Du Jian-Guo(杜建国)[a)]

[a)] *Key Laboratory of Earthquake Prediction, Institute of Earthquake Science, China Earthquake Administration, Beijing* 100036, *China*
[b)] *Institute of Microstructure and Properties of Advanced Materials, Beijing University of Technology, Beijing* 100124, *China*

(Received 23 July 2015; revised manuscript received 21 August 2015; published online 20 October 2015)

The crystal structure and Raman spectra of quartz are calculated by using first-principles method in a pressure range from 0 to 5 GPa. The results show that the lattice constants (a, c, and V) decrease with increasing pressure and the a-axis is more compressible than the c axis. The Si–O bond distance decreases with increasing pressure, which is in contrast to experimental results reported by Hazen *et al.* [Hazen R M, Finger L W, Hemley R J and Mao H K 1989 *Solid State Communications* **725** 507–511], and Glinnemann *et al.* [Glinnemann J, King H E Jr, Schulz H, Hahn T, La Placa S J and Dacol F 1992 *Z. Kristallogr.* **198** 177–212]. The most striking changes are of inter-tetrahedral O–O distances and Si–O–Si angles. The volume of the SiO_4^{4-} tetrahedron decreased by 0.9% (from 0 to 5 GPa), which suggests that it is relatively rigid. Vibrational models of the quartz modes are identified by visualizing the associated atomic motions. Raman vibrations are mainly controlled by the deformation of the SiO_4^{4-} tetrahedron and the changes in the Si–O–Si bonds. Vibrational directions and intensities of atoms in all Raman modes just show little deviations when pressure increases from 0 to 5 GPa. The pressure derivatives ($d\nu_i/dP$) of the 12 Raman frequencies are obtained at 0 GPa–5 GPa. The calculated results show that first-principles methods can well describe the high-pressure structural properties and Raman spectra of quartz. The combination of first-principles simulations of the Raman frequencies of minerals and Raman spectroscopy experiments is a useful tool for exploring the stress conditions within the Earth.

Keywords: structural properties, Raman mode, quartz, first principles

PACS: 74.25.nd, 62.50.–p, 63.20.dk **DOI:** 10.1088/1674-1056/24/12/127401

1. Introduction

Vibrational property of mineral as a function of pressure, temperature, and composition has many applications in geosciences. Mechanical, elastic properties and phase transitions of materials can be studied by probing the vibrational dynamics. High-pressure Raman spectra are useful in characterizing materials of geological and geophysical interest. The analysis of vibrational spectra may be conducive to the understanding of the thermodynamic properties of solids at pressures that are beyond the range of direct thermochemical measurements.

Quartz is the second most abundant mineral after feldspar in the continental crust. Therefore, vibrational spectrum of quartz has been extensively studied.[1,2] For example, the room temperature high-pressure Raman modes of quartz[3–7] and the temperature dependence of the Raman spectra of quartz at atmospheric pressure[1,4,8–13] were investigated experimentally. Nevertheless, there are evident discrepancies among the different studies.

Theoretical simulations can establish a link between the experimentally observed peaks in the spectra and the underlying atomic dynamics and structure. First principles methods have been successfully applied to geosciences and material science.[14–19] They have also been used in calculating the Raman spectroscopic properties of SiO_2.[20,21] However, first-principles investigations of the high-pressure Raman spectra of quartz are rarely reported. This study aims to fill this gap by investigating the lattice deformation, and the structural and Raman spectral properties of quartz at high pressure using first-principles simulations.

2. Computational method

Quartz belongs to the trigonal crystal system. It has two enantiomorphs with space groups $P3_121$ and $P3_221$, respectively, and nine atoms per unit cell ($Z = 3$).[22] Quartz is made of a continuous framework of Si–O tetrahedron (SiO_4^{4-}) and each oxygen atom is shared by two tetrahedrons (Fig. 1). The ideal crystal shape is of a sixsided prism terminating at six-sided pyramids at each end.

Vibrational spectra of crystalline solids can be interpreted by using the factor group analysis.[23] The irreducible representation of the optical vibrations of quartz for the D_3 factor group is written as

$$\Gamma_{\rm op} = 4A_1 + 4A_2 + 8E,$$

*Project supported by the Key Laboratory of Earthquake Prediction, Institute of Earthquake Science, China Earthquake Administration (CEA) (Grant No. 2012IES010201) and the National Natural Science Foundation of China (Grant Nos. 41174071 and 41373060).

†Corresponding author. E-mail: liulei@cea-ies.ac.cn

© 2015 Chinese Physical Society and IOP Publishing Ltd

where A_1 is the Raman-active mode, A_2 is the infrared-active mode, and E is the Raman- and infrared-active mode.

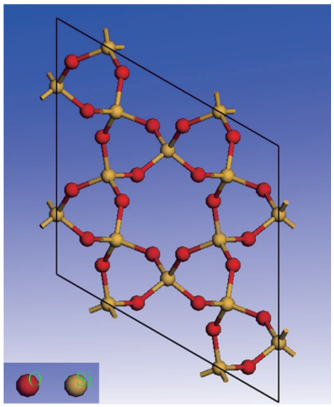


Fig. 1. (color online) Atomic structure of quartz crystal (view from (001)).

First-principles calculations were performed by using the density functional perturbation theory (DFPT),[24] the density functional theory (DFT),[25,26] and the plane-wave pseudopotential technique as implemented in the CASTEP code.[27] Local density approximation (LDA) with CA–PZ parameterization[28,29] was used for describing the exchange-correlation interaction. Norm-conserving pseudopotentials[30] were used to model the electron-ion interaction. A $6 \times 6 \times 5$ Monkhorst–Pack grid of k points was adopted for sampling the Brillouin zone. The total-energy convergence criterion of 5×10^{-7} a.u. (The unit a.u. is short for arbitrary units) was used in the self-consistent field calculations. The energy cut-off for the plane-wave basis was chosen to be 830 eV.

Within the plane-wave pseudopotential framework, the unit-cell stress tensor can be directly calculated by using the stress theorem.[31] The structure and Raman spectroscopic properties of quartz at pressure were calculated by simultaneously optimizing the lattice constants and atomic positions based on the principle that the Hellmann–Feynman forces and stresses act on the nuclei, and the lattice parameters were minimized.[31] The convergence criteria for the force and stress are 0.01 eV/Å and 0.02 GPa, respectively.

The spatial derivatives of the macroscopic polarization were numerically calculated along the eigenvectors of each Raman active phonon mode by calculating the polarization for each displacement through using the linear response formalism.[32] Once these derivatives are known, the Raman cross section can be calculated through appropriate space averaging. Computational and theoretical details of Raman spectra by using DFT can be found in the work of Porezag and Pederson[33] and Refson, *et al.*[24]

3. Results and discussion

3.1. Benchmark calculation

To assess the performances of the DFT and DFPT total-energy approach used here, test calculations of the cell parameters, elastic constants and frequencies of the Raman spectra of quartz are carried out under 0 K.

The differences between the calculated values of cell volumes, lattice parameters a and c and experimentally measured corresponding values[22,34–37] are 3.7%, 1.3%, and 1.1%, respectively. The inter- and intra-tetrahedral distances, angles, and volume of SiO_4^{4-} tetrahedron are listed in Table 1. The

Table 1. Selected interatomic distances and angles of quartz under ambient condition.

			Intra-tetrahedral distance/Å				Δ/%
Si–O×2	1.605	1.605	1.607	1.607	1.606	1.602	0.25
Si–O×2	1.611	1.614	1.613	1.611	1.614	1.607	0.35
Average	1.608	1.61	1.61	1.609	1.61	1.605	0.27
O–O		2.645	2.648		2.64	2.639	0.20
O–O		2.617	2.618		2.621	2.612	0.25
O–O		2.631	2.628		2.637	2.623	0.34
O–O		2.612	2.613		2.615	2.602	0.43
Average		2.626	2.627		2.628	2.619	0.31
			Inter-tetrahedral distance/Å				
Si–Si		3.0585	3.059		3.062	3.025	1.14
O–O		3.411	3.414		3.414	3.300	3.31
O–O		3.331	3.335		3.033	3.199	1.05
			Intra-tetrahedral angles/(°)				
O–Si–O×2	110.26	110.52	110.7	110.39	110.19	110.71×2	0.27
O–Si–O×2	108.729	108.81	108.8	108.7	108.69	108.38×2	0.34
O–Si–O	109.16	108.93	109.1	109.07	109.6	109.43	0.24
O–Si–O	109.47	109.24	108.8	109.57	109.5	109.24	0.07
Average	109.47	109.38	109.35	109.47	109.48	109.44	0.1
			Inter-tetrahedral angles/(°)				
Si–O–Si	143.84	143.73	143.6	143.68	144.2	141.073	1.9
V (SiO_4^{4-}) (Å^3)		2.138	2.138		2.139	2.118	0.97
Reference	[34]	[35]	[36]	[22]	[37]	This work	

Notes: Δ is the difference between this calculation value and previous experimental result.

differences between calculated and experimental values of intra-tetrahedral distances (Si–O and O–O) are less than 0.5%. The differences between the calculated inter-tetrahedral distances (Si–Si and O–O) and the experimental values are 1.14% and 3.31%, respectively. Furthermore, the differences between the calculated and experimental intra-tetrahedral angles (O–Si–O angle) are less than 0.35% and the difference between the calculated and experimental inter-tetrahedral angles (Si–O–Si angles) is 1.9%. The calculated volume of the SiO_4^{4-} tetrahedron agrees with the previous experimental result and their difference is 0.97%.

The elastic constants are calculated by using the stress-strain approach. A total of 6 strains (−0.005, −0.003, −0.001, 0.001, 0.003, 0.005) are used in calculating. Our DFT calculation reproduces the quartz elastic constants reasonably well under ambient condition (Table 2). The Raman frequencies of quartz are calculated at 0 GPa and compared with the experimental data to evaluate the performances of the DFT and DFPT method. The calculated frequencies show good agreement with previous experimental values (Table 3). The differences between the calculated and experimental frequencies[2,4,5] are less than 4.1% (mostly less than 1%), with the exception of 8.4% for the 206 cm^{-1} mode. This bigger difference (8.4%) may come from the effect of pressure. The pressure derivative ($d\nu_i/dP$) of 206 cm^{-1} mode is the biggest (18.6 cm^{-1}/GPa as shown below) in all the modes of quartz, and we obtain the frequency under 0 GPa, but the experimental results are acquired under atmospheric conditions.

Table 2. Some reported elastic parameters of quartz crystals under ambient condition.

	Eleatic constant				
C_{11}	87.26	81.1	86.8	87.7	81.7
C_{33}	105.8	104.8	106.4	106.3	99.5
C_{44}	57.15	49.7	58	59	59.3
C_{66}	40.35	36.4	39.8	40.5	37.2
C_{12}	6.57	8.3	7.2	6.8	7.3
C_{13}	11.95	7.5	12	12.3	11.0
C_{14}	17.18	23.3	17.9	18.7	14.3
K	37.67	34.4	37.5	37.8	35.5
G	46.91				44.0
Reference	[38]	[39]	[39]	[40]	this work

For checking the precision of calculated plan, the structure, elastic constant and Raman frequency under higher energy cutoffs with 900 eV, 950 eV, 1000 eV, 1050 eV, 1100 eV, and 1200 eV are calculated. The calculations show the differences among lattice constants and among volumes are both smaller than 0.01%. The average difference of bulk modulus and shear modulus with different energy cutoffs are 4.8% and 2.2%, respectively. Differences among all Raman frequencies are all smaller than 1 cm^{-1} with different energy cutoffs (830 eV, 900 eV, 950 eV, 1000 eV, 1050 eV, 1100 eV, and 1200 eV).

Consequently, the close agreement between the experimental and calculated values of lattice parameters, elastic properties and Raman frequencies demonstrate the validity of the computational scheme.

Table 3. Frequencies of the Raman spectrum of quartz.

Symmetry	Frequency (ν_i)/cm^{-1}				Δ/%
A_1	206	207	205.9	223.6	8.4
	355	356	355.6	340.8	4.1
	464	464	464.1	459.1	1.1
	1085	1085	1084.5	1085.3	0.
E(LO + TO)	128	128	127.9	129.7	1.4
(LO + TO)	265	265	264.6	258.2	2.5
(LO + TO)	696	697	696	694.7	0.2
(LO + TO)	1162	1162	1161.5	1152.6	0.8
E(TO)	394	394	394.1	378.6	3.9
(LO)	401	401	401		
(TO)	450	450	450.2	440.8	2.1
(LO)	511	509	510.6		
(TO)	796	795	795.7	796.7	0.1
(LO)	808	807	807.8		
(TO)	1069	1072	1069.4	1069.0	0.1
(LO)	1230	1231	1230		
Reference	[5]	[2]	[4]	this work	

Note: Δ is the difference between the calculation and previous experimental result.

3.2. Pressure effect on the quartz crystal structure

3.2.1. Lattice parameters and pressure

The structural properties of quart are calculated in a pressure range from 0 to 5 GPa in this work. The quartz transforms into coesite at about 2 GPa,[41] then transform into stishovite at 8 GPa,[42] and then transform into CaCl2-structure phase at 51 GPa,[43] and then transform into α-PbO2-structure phase at 98 GPa.[44] Though the pressure up to 5 GPa, no phase transitions happen in this study because the simulated temperature is 0 K.

Lattice parameters (a, c, and V) are fitted with a pressure-dependent quadratic function (Eq. (1))

$$M = M_0 + M_1 P + M_2 P^2, \tag{1}$$

where M denotes the lattice parameters (a, c, and V), P denotes the pressure, and M_i ($i = 0, 1, 2$) are the fitting coefficients.

The variations of lattice parameters with pressure are shown in Fig. 2. The calculated and experimental data are fitted with Eq. (1) and the results are listed in Table 4. The calculated lattice constants show better agreement with previous experimental results. The a and c reduce 3.9% and 2.4% with pressure increasing from 0 to 5 GPa. So the a axis is more compressible than the c axis.

Table 4. Quadratic fitting of lattice parametes (a, c, and V) when pressure increase from 0 GPa to 5 GPa.

a			c			V			Reference
M	M_1	M_2	M	M_1	M_2	M	M_1	M_2	
4.914	–0.0577	0.0034	5.406	–00452	0.0029	113.06	3.5466	0.2183	[36]
4.921	–0.0397	0.0008	5.416	–0.0335	0.0014	113.59	–2.4886	0.0715	[37]
4.917	–0.0455	0.0018	5.406	–0.0362	0.002	113.18	–2.815	0.132	[35]
4.850	–0.048	0.002	5.348	–0.037	0.002	108.94	–2.895	0.156	this work

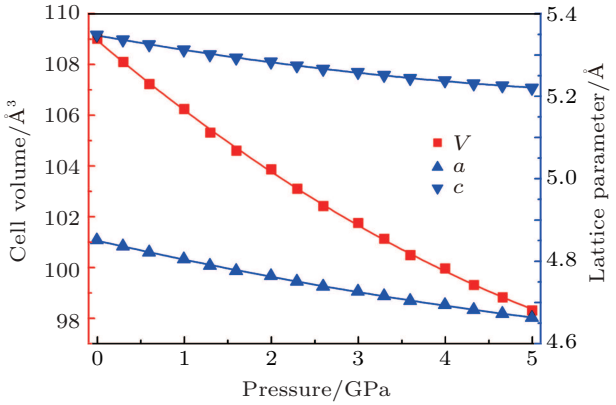


Fig. 2. (color online) Variations of lattice parameter with pressure of quartz.

3.2.2. Variations of bond length and bond angle with pressure

The intra-tetrahedral bond (O–O and Si–O distance) and bond angle (O–Si–O angle) both vary with pressure but not in the same manner (Figs. 3–5).

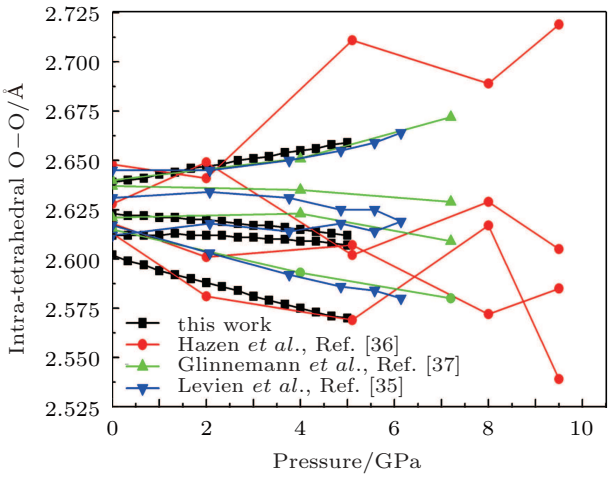


Fig. 3. (color online) Changes of intra-tetrahedral O–O distance with pressure.

The calculated results suggest four different intra-tetrahedral O–O distances in quartz (Fig. 3). The longest one increases linearly with increasing pressure, whereas the shortest one decreases linearly with increasing pressure and the rest decrease slightly. These variations completely agree with the experimental results.[35–37] The difference between the longest and shortest O–O distances increases with increasing pressure as indicated by the increase in the SiO_4^{4-} tetrahedral distortion under high pressure. But the calculated O–O distances do not agree well with the results of Hazen *et al.*[36]

The Si–O bond lengths at different pressures are shown in Fig. 4. The larger Si–O bond length slightly decreases from 1.607 Å to 1.604 Å and the shorter Si–O length decreases from 1.602 Å to 1.596 Å as pressure increases when the pressure increases from 0 to 5 GPa. The values of the larger Si–O length remains constant up to 10 GPa,[37] whereas Levien *et al.*[35] reported that the larger Si–O length decreased and Hazen *et al.*[36] reported that the larger Si–O length increased with increasing pressure. The calculated results agree with the experimental data of Levien *et al.*[35] All the shorter Si–O distances show decreasing with increasing pressure.

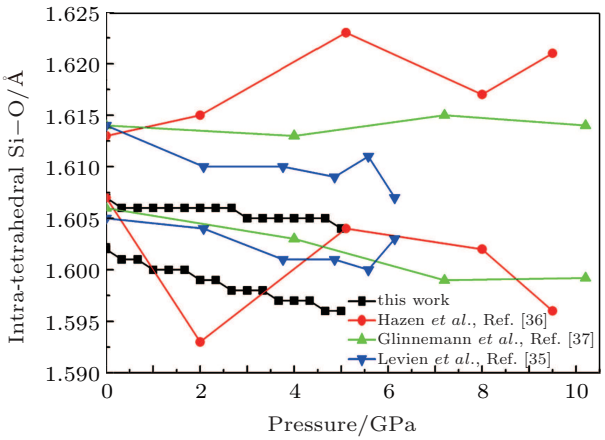


Fig. 4. (color online) Changes of intra-tetrahedral Si–O distance with pressure.

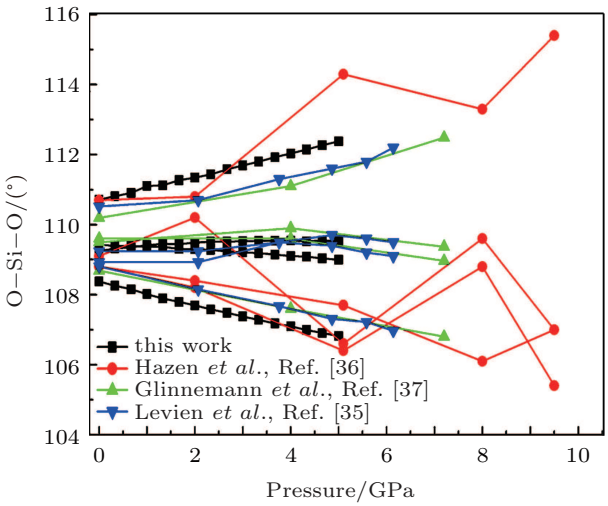


Fig. 5. (color online) Changes of intra-tetrahedral O–Si–O angle with pressure.

The largest O–Si–O angle linearly increases with increasing pressure, whereas the smallest one linearly decreases with

increasing pressure. The calculated changes of O–Si–O angles in the $SiO4^{4-}$ tetrahedron with pressure well agree with the experimental results,[35,37] however they are different from the results obtained by Hazen, *et al.*[36] The variations of O–Si–O angles with pressure show similar manners to those of intra-tetrahedral O–O distances. The differences between O–O distances and between O–Si–O angles increase with increasing pressure and suggest that the SiO_4^{4-} tetrahedral distortion increases with increasing pressure. The changes of the intra-tetrahedral O–O distances, Si–O distances and O–Si–O angles with increasing pressure suggest that the O–Si–O angle variation depends on the O–O distance but not on the Si–O distance, which agrees with the regression results of Glinnemann *et al.*[37]

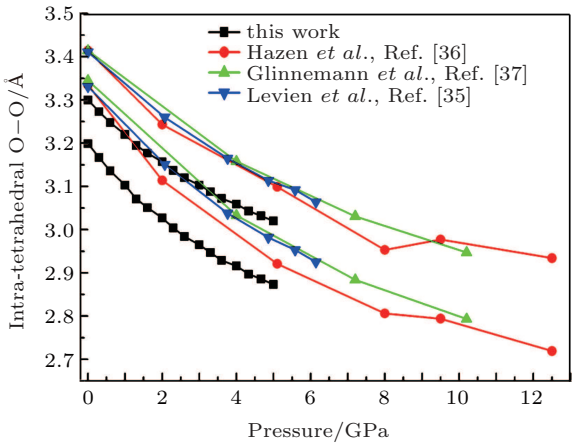


Fig. 6. (color online) Changes of inter-tetrahedral O–O length with pressure.

The inter-tetrahedral features of O–O and Si–Si distances and Si–O–Si angles at high pressures are calculated. The two shortest O–O distances between the SiO_4^{4-} tetrahedra are measured (Fig. 6). The difference between the two O–O distances slightly increases with increasing pressure. The shortest inter-tetrahedral O–O distance at 0 GPa is approximately 3.199 Å, which is significantly larger than the 2.619 Å, the average value of the intra-tetrahedral O–O distance.

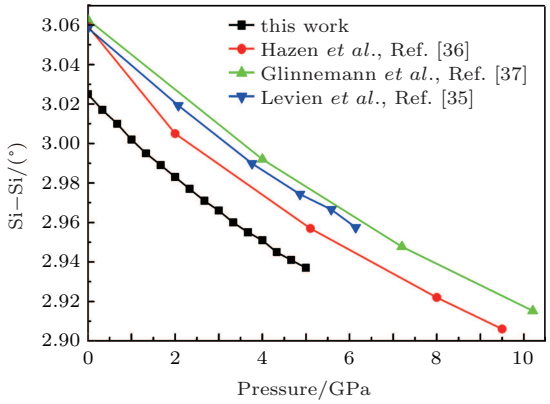


Fig. 7. (color online) Changes of inter-tetrahedral Si–Si length with pressure.

The correlation of the calculated and experimental[35–37] Si–Si distance with pressure is shown in Fig. 7. Though the calculated values are smaller than the experimental values, the decreasing rates are similar. Figure 8 shows the variations of Si–O–Si angle data with pressure. The Si–O–Si angle obviously decreases with increasing pressure. The SiO_4^{4-} tetrahedron volume decreases by 0.9% when the pressure increases from 0 GPa to 5 GPa (Fig. 9), which suggests that it is relatively rigid.

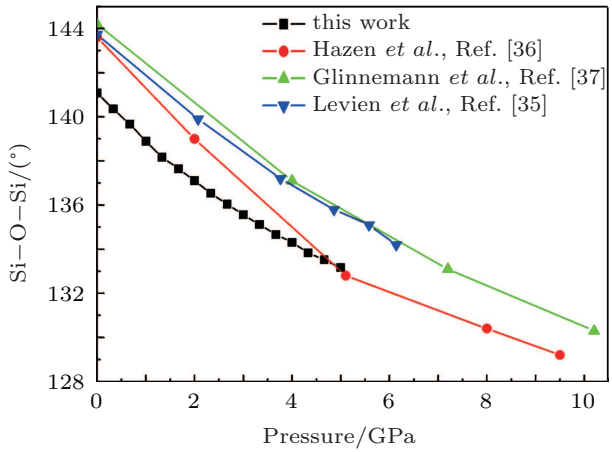


Fig. 8. (color online) Changes of inter-tetrahedral Si–O–Si angle with pressure.

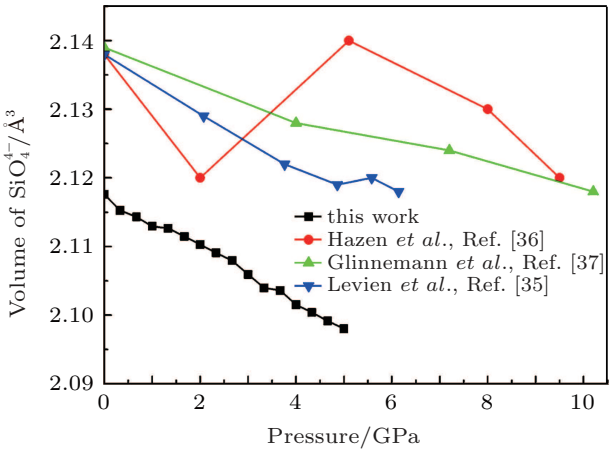


Fig. 9. (color online) Changes of volume of SiO_4^{4-} tetrahedron with pressure.

The quartz cell volume decreases by 9.8% when the pressure increases from 0 GPa to 5 GPa. Most of oxide crystals are compressed by two principle structural mechanisms: the shortening of the metal–oxygen distances and the decreasing of metal–oxygen–metal angles.[45,46] The intra-tetrahedral Si–O distance decreases by 0.3% and the volume of the SiO_4^{4-} tetrahedron decreases by 0.9% when the pressure increases from 0 GPa to 5 GPa. However, the inter-tetrahedral O–O and Si–Si distances, and Si–O–Si angles decrease by 8.5%, 10.2%, 2.9%, and 5.6% when the pressure increases from 0 GPa to 5 GPa, respectively. The most striking changes are the variations of inter-tetrahedral O–O distances and Si–O–Si angles.

Hence, quartz is compressed because the inter-tetrahedral distances and angles decrease.

3.3. Vibrational pattern of Raman modes

The vibrational patterns of quartz Raman modes are identified by visualizing the associated atomic motion with the aid of animation of the computed vibrational modes that were built in the CASTEP package and shown in Fig. 10, respectively.

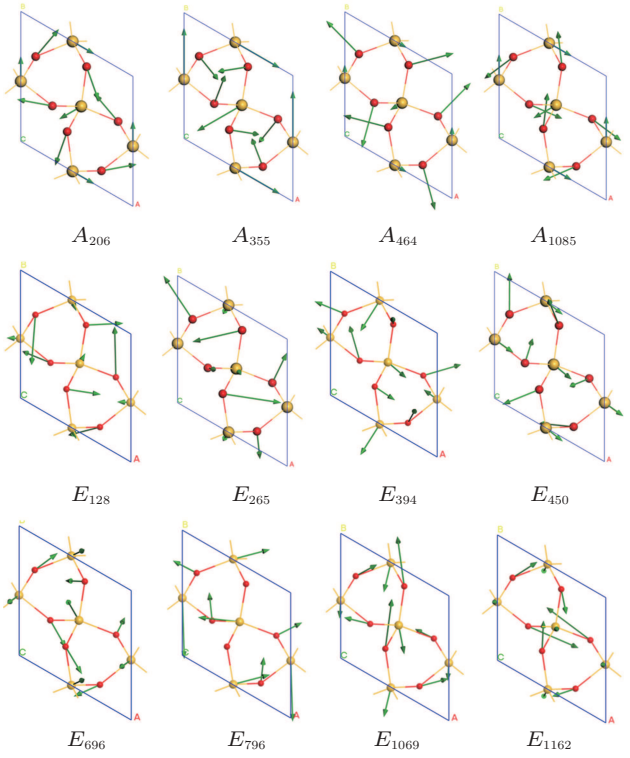


Fig. 10. (color online) Schematic diagrams of vibrational model of quartz Raman mode (view from (001)). The arrow and its length indicate the direction of atomic motion and vibrational intensity.

All A_1 modes have the same Si atom vibrational directions and different vibrational intensities. The directions of Si atom translation within crystal plane are parallel to the [100], [010], and [110] directions. The A_{355} mode has the strongest Si vibrational intensity and the A_{464} mode has the lowest vibrational intensity. For the O atom movement, the A_{355} and A_{464} modes have similar atomic vibrational intensities and opposite vibrational directions. The A_{206} and A_{1085} modes have similar atomic vibrational intensities and opposite vibrational directions. The vibrational intensities of the Si and O atoms in the A_{208} and A_{1085} modes are nearly identical. In the A_{464} mode, the vibrational intensity of the O atom is much larger than that of the Si atom; however, in the A_{355} mode, the vibrational intensity of the Si atom is much larger than that of the O atom. The E modes have complex and different vibrational modes.

The differences in direction and intensity among the different modes are attributed to the differences between the Si and O atom motions. Except for the E_{796} and A_{464} modes, the intensity of the O atomic vibration is larger than that of Si. The results suggest that the Raman vibration in quartz is mainly controlled by the deformation of the SiO_4^{4-} tetrahedron and the variation of Si–O–Si angle. The vibrational directions and intensities of atoms in all Raman modes just show little deflection when pressure increases from 0 GPa to 5 GPa.

3.4. Pressure dependence of the quartz Raman frequencies

Raman shifts for the 12 frequencies of quartz are obtained at different pressures from 0 GPa to 5 GPa (Figs. 11 and 12). The calculated and experimental values for the pressure derivatives (dv_i/dP) from 0 GPa to 5 GPa are listed in Table 5. The mode of the Raman spectrum of quartz can be roughly classified as two categories in terms of their pressure dependences. The frequencies in the first group are nearly independent of pressure (pressure derivative < 1 cm^{-1}/GPa). This category includes A_{355} and A_{1086} modes, which are associated with A_1 symmetry, and E_{394} and E_{1069} modes, which are associated with E symmetry. The E_{1162} mode (pressure derivative $= -2.3$ cm^{-1}/GPa) also may belong to this group. The second group consists of whose frequencies that change significantly with increasing pressure (pressure derivative > 3 cm^{-1}/GPa). This group includes the A_{206} and A_{464} modes of A_1 symmetry and E_{128}, E_{265}, E_{450}, E_{696}, and E_{796} modes of E symmetry. The pressure derivatives of E_{394}, E_{1069}, and E_{1162} modes are negative with values of -0.2, -0.6, and -2.3 cm^{-1}/GPa, respectively. The negative pressure shifts suggest the weakening of the structure along these normal coordinates.[5] The other modes have positive pressure derivatives.

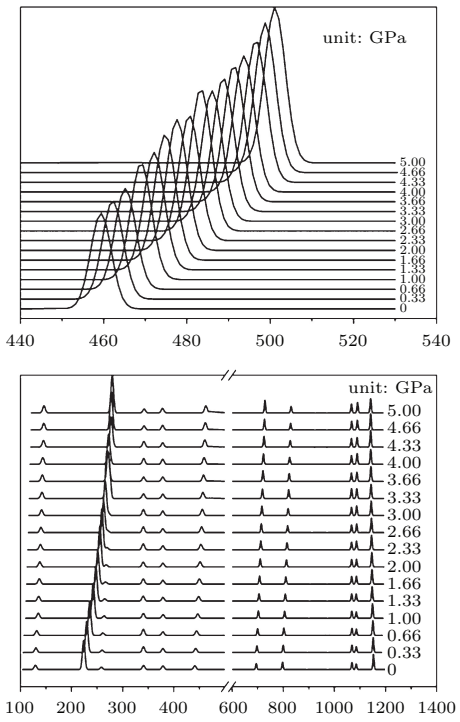


Fig. 11. Raman spectra of quartz as a function of pressure.

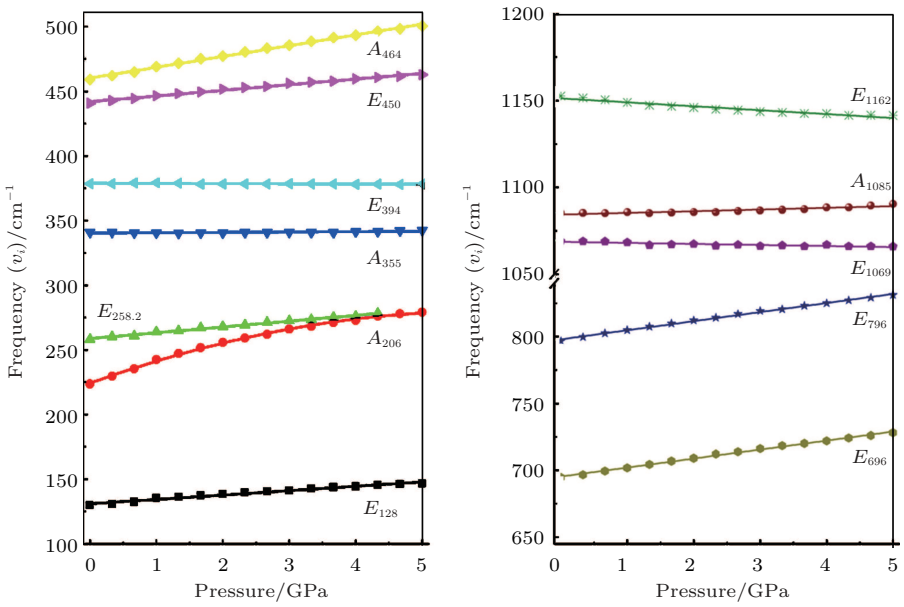


Fig. 12. (color online) Pressure dependences of quartz Raman frequency.

Table 5. Pressure shifts of the Raman modes of quartz.

Symmetry		Mode/cm^{-1}	(dν_i/dP)/(cm^{-1}/GPa)						Mode/cm^{-1}	(dν_i/dP)/(cm^{-1}/GPa)
		206	19.9	18	20	21.3		24	223.6	18.6
A	A_1	355	–1.2			–0.3		0.5	340.8	0.3
		464	8	9	8.1	8	8.44	8	459.1	8.4
		1085	1.4			1.5			1085.3	1.0
	E(LO + TO)	128	5.5	5	5.4	5.8		6	129.7	3.4
E	(LO + TO)	265	3.5			4.8		6	258.2	4.5
	(LO + TO)	696	7	8		9.6			694.7	6.8
	(LO + TO)	1162	–3.1			–2.6			1152.6	–2.3
	E(TO)	394	–0.09			0.9			378.6	–0.2
	(LO)	401								
	(TO)	450	4.6			8.2		5	440.8	4.4
E	(LO)	511								
	(TO)	796	5.9	8		10.9			796.7	6.8
	(LO)	808								
	(TO)	1069	1			2			1069.0	–0.6
	(LO)	1230								
Reference			[5]	[3]	[4]	[47]	[11]	[6]	this work	

The A_{206} mode is strongly anharmonic[9,10] and has the largest pressure derivative. The frequency shift of this mode with pressure is about 3 times greater than that of the ruby fluorescence lines. This mode can be used as an alternative pressure sensor to the ruby fluorescence technique for experiments at room temperature at pressures from 0 Gpa to approximately 5 GPa. The modes are likely to have large contribution from Si–O stretching motions, rotations of the Si–O–Si angles and SiO_4^{4-} tetrahedron. The A_{464} mode is the strongest vibrational line and has larger pressure derivative. It used to be a pressure sensor in the high pressure experiment. The Si–O bond stretching motion and rotation of the SiO_4^{4-} tetrahedron control the vibration of this mode. The other modes involve complex translations, rotations and deflection of Si–O bond, Si–O–Si angles and SiO_4^{4-} tetrahedron. But we cannot conclude the reason of pressure derivative difference among different Raman modes from the vibrations of Si and O atom in quartz.

Nonetheless, the experimental pressure derivatives of the Raman frequencies are different among the various studies. The calculated results fall within the scope of previously reported experimental data. Presumably, the calculations may serve as reference and supplement the experiments.

4. Conclusions and implication

The structural and Raman vibrational properties of quartz are calculated by first principles method. Lattice constants (a,

c, and V) are quadratic and fitted as a function of pressure and a axis is more compressible than c axis. So the differences between intra-tetrahedral O–O distances and between O–Si–O angles increase with pressure increasing, indicating that the SiO_4^{4-} tetrahedral distortion increases under high pressure. Si–O distance decreases with increasing pressure, which is different from previous results.[36,37]

The inter-tetrahedral O–O and Si–O lengths and Si–O–Si angle decrease with increasing pressure. The shortest inter-tetrahedral O–O distance at 0 GPa is 3.199 Å, which is significantly larger than 2.619 Å, the average value of intra-tetrahedral O–O distance. Volume of SiO_4^{4-} tetrahedron decreases by 0.9% when pressure increases from 0 GPa to 5 GPa (Fig. 9), indicating that it remains relatively rigid under high pressure. The changes of interatomic distance and angel of quartz with pressure show that the most striking changes happen to the inter-tetrahedral O–O distances and then Si–O–Si angles. So the compression of quartz obviously results from the decreases of inter-tetrahedral distance and angle.

Raman frequency and vibrational model of each mode of quartz are calculated under pressures ranging from 0 GPa to 5 GPa. Raman vibrational model shows that the Raman vibration of quartz is mainly controlled by deformation of SiO_4^{4-} tetrahedron and change of Si–O–Si bond. The vibrational directions and intensities of atom of all modes have little changes, but the general vibrational properties of each mode remain unchanged when pressure increases from 0 GPa to 5 GPa. The 206 cm^{-1} and 464 cm^{-1} A mode and the 128, 265, 450, 696, and 796 cm^{-1} E mode have larger positive pressure derivative values and 355 cm^{-1} A mode and E_{394} mode keep nearly unchanged under high pressures. However the $E_{378.6}$, E_{1069}, and $E_{1152.6}$ modes have negative pressure derivatives. The calculated results show that the first principles method can well describe the property structure and Raman spectra of quartz under high pressures.

The spectra of elemental excitations vary with pressure, thus the associated phenomena can be effectively studied by in situ Raman spectra. The study of the changes in the Raman frequency of quartz at high pressure can help understand the stress conditions in the Earth's interior. Metamorphic pressures are assessed by using Raman spectra in quartz eclogites, epidote amphibolites, and amphibolite facie rocks with estimated residual pressures of 0.8 GPa–1.0 GPa, 0.4 GPa–0.6 GPa, and 0.1 GPa–0.2 GPa, respectively. Apparently, Raman spectrum analysis of quartz is an effective and simple method of investigating the pressure conditions in metamorphic rocks.[48] We measured the shift of the Raman 464 cm^{-1} vibrational mode in quartz grains from the Wenchuan earthquake fault zone and found that the stress near the fault plane was about 368 MPa.[49] Furthermore, the method can also be used in calcite, feldspar, olivine and other minerals from faults, tectonic boundaries, and mantle rocks, and this method is probably very useful when minerals are preserved in inclusions for understanding the stress condition of fault and tectonic interior. The first-principles simulations can help to quantify the pressure-dependent variations in the Raman frequencies of minerals. The combination of first-principles simulations and Raman spectroscopy experiments is a great exploration tool of terrestrial stress conditions

References

[1] Raman C V and Nedungadi T M K 1940 *Nature* **145** 147
[2] Scott J F and Porto S P S 1967 *Phys. Rev.* **161** 903
[3] Asell J F and Nicol M 1968 *J. Chem. Phys.* **49** 5395
[4] Dean K J, Sherman W F and Wilkinson G R 1982 *Spectrochim. Acta* **38A** 1105
[5] Hemley RJ 1987 "Pressure dependence of Raman spectra of SiO_2 polymorphs: α-quartz, coesite, and stishovite", in Manghnani M H and Syono Y, eds., *High-Pressure Research in Mineral Physics* (Tokyo-AGU, Washington, D.C.: Terrapub)
[6] Jayaraman A, Wood D L and Maines R G 1987 *Phys. Rev. B* **35** 8136
[7] Liu L and Mernagh T P 1992 *High Temperatures-High Pressures* **24** 13
[8] Bates J B and Quist A S 1972 *J. Chem. Phys.* **56** 1528
[9] Castex J and Madon M 1995 *Phys. Chem. Minerals* **22** 1
[10] Gillet P, Le Cléach A and Madon M 1990 *J. Geophys. Res.* **95** 21635
[11] Schmidt C and Ziemann M A 2000 *Am. Mineral* **85** 1725
[12] Shapiros M, O'Shen D C and Cummins H Z 1967 *Phys. Rev. Lett.* **19** 361
[13] Bist H D, Durig J R and Sullivan J F 1989 *Raman spectroscopy: Sixty years on vibrational spectra and structure* (Amsterdam: Elsevier)
[14] Gillan M J, Alfe D, Brodholt J, Vocadlo L and Price G D 2006 *Rep. Prog. Phys.* **69** 2365
[15] Jahn S and Kowalski P 2014 *Reviews in Mineralogy & Geochemistry* **781** 691
[16] Peng Q, He C Y, Li J and Zhong J X 2015 *Acta Phys. Sin.* **64** 047102 (in Chinese)
[17] Wang J M, Hu J P, Liu C H and Ouyang C Y 2012 *Physics* **41** 95 (in Chinese)
[18] Zhang P, Kong C and Zheng C 2015 *Chin. Phys. B* **24** 024221
[19] Wei Z, Zhai D and Shao X H 2015 *Chin. Phys. B* **24** 043102
[20] McMillan P F and Hess A C 1990 *Phys. Chem. Minerals* **17** 97
[21] Dračinskỳ M Benda L and Bouř P 2011 *Chem. Phys. Lett.* **512** 54
[22] Le Page Y and Donnay G 1976 *Acta Cryst.* **32** 2456
[23] Fateley WG, Dollish F R, Mcdevitt N T and Bentley F F 1972 *Infrared and Raman Selection Rules for Molecular and Lattice Librations: The Correlation Method* (New York: Wiley-Interscience)
[24] Refson K, Tulip P R and Clark S J 2006 *Phys. Rev. B* **73** 155114
[25] Kohn W and Sham L J 1965 *Phys. Rev. A* **140** 1133
[26] Hohenberg P and Kohn W 1964 *Phys. Rev. B* **136** 864
[27] Clark S J, Segall M D, Pickard C J, Hasnip P J, Probert M J, Refson K and Payne M C 2005 *Z. Kristallogr.* **220** 567
[28] Ceperley D M and Alder B J 1980 *Phys. Rev. Lett.* **45** 566
[29] Perdew J P and Wang Y 1992 *Phys. Rev. B* **45** 13244
[30] Hamann D R, Schluter M and Chiang C 1979 *Phys. Rev. Lett.* **43** 1494
[31] Nielsen O H and Martin R M 1983 *Phys. Rev. Lett.* **50** 697
[32] Gonze X 1997 *Phys. Rev. B* **55** 10337
[33] Porezag D and Pederson M R 1996 *Phys. Rev. B* **54** 7830
[34] Antao S M, Hassan I, Wang J, Lee P L and Toby B H 2008 *The Canadian Mineralogist* **46** 1501
[35] Levien L, Prewitt C T and Weidner D J 1980 *Am. Mineral* **65** 920

[36] Hazen R M, Finger L W, Hemley R J and Mao H K 1989 *Solid State Commun.* **725** 507
[37] Glinnemann J, King H E Jr, Schulz H, Hahn T, La Placa S J and Dacol F 1992 *Z. Kristallogr.* **198** 177
[38] Heyliger P, Ledbetter H and Kim S 2003 *J. Acoust. Soc. Am.* **142** 644
[39] Kimizuka H, Ogata S, Li J and Shibutani Y 2007 *Phys. Rev. B* **75** 054109
[40] Zubov V and Firsova M 1962 *Sov. Phys. Crystallogr.* **7** 374
[41] Liu L G and Bassett W A 1986 *Element, oxides and silicates, high pressure phases with implications for the Earth's interior* (New York: Oxford University Press)
[42] Bose K and Ganguly J 1995 *Am. Mineral* **80** 231
[43] Ono S, Hirose K, Murakami M and Isshiki M 2002 *Earth Planet Sci. Lett.* **197** 187
[44] Murakami M, Hirose K, Ono S and Ohishi Y 2003 *Geophys. Res. Lett.* **30** 1207
[45] Ohno I 1995 *J. Phys. Earth* **43** 157
[46] Hazen RM and Finger W 1985 *Sci. Am.* **252** 110
[47] Briggs R J and Randis A K 1977 *Phys. Rev. B* **16** 3815
[48] Enami M, Nishiyama T and Mouri T 2007 *Am. Mineral* **92** 1303
[49] Xie C, Zhou B and Liu L 2015 *Spectroscopy and Spectral Analysis* **351** 118 (in Chinese)